In-Plane Stress and Displacement Distributions in a Spinning Annular Disk Under Stationary Edge Loads

Jen-San Chen
Associate Professor.

Jhi-Lu Jhu
Graduate Student.

Department of Mechanical Engineering,
National Taiwan University
Taipei, Taiwan 107,
Republic of China

It is well known that the in-plane stress and displacement distributions in a stationary annular disk under stationary edge tractions can be obtained through the use of Airy stress function in the classical theory of linear elasticity. By using Lame's potentials, this paper extends these solutions to the case of a spinning disk under stationary edge tractions. It is also demonstrated that the problem of stationary disk-spinning load differs from the problem of spinning disk-stationary load not only by the centrifugal effect, but also by additional terms arising from the Coriolis effect. Numerical simulations show that the amplitudes of the stress and displacement fields grow unboundedly as the rotational speed of the disk approaches the critical speeds. As the rotational speed approaches zero, on the other hand, the in-plane stresses and displacements are shown, both numerically and analytically, to recover the classical solutions derived through the Airy stress function.

Introduction

Designers of spur gears, grinding wheels, and circular saw blades are often interested in the dynamic stresses induced in a rotating disk under space-fixed in-plane edge loads. In gearboxes and grinding wheels, the in-plane vibration is transmitted through the bearing to the machine casing, where it may produce unwanted noise. In the wood cutting industry, it is well known that the bending vibration and stability of the spinning disk are significantly affected by the in-plane stress distribution induced by the cutting forces on the outer rim (Chen, 1994; Shen and Song, 1996). In these analyses, the in-plane stress distribution is obtained, in additional to the components due to the centrifugal effect, by assuming that both the disk and the edge load are fixed in space. This assumption is acceptable when the rotation speed of the disk is relatively low. In the very high speed range, on the other hand, it is not certain whether it is appropriate to ignore the effect of relative motion between the spinning disk and the space-fixed edge load on the in-plane stress distribution.

It is well known that the natural frequencies of the in-plane radial and torsional vibrations of a spinning disk depend on the rotation speed. Bhuta and Jones (1963) investigated the axisymmetric planar vibration of a rotating full disk and found that the effect of rotation is generally to lower the natural frequencies. The same problem was studied by Doby (1969) with different formulation. Burdess et al. (1987) generalized the analysis to asymmetric in-plane vibration, and discussed the properties of both the forward and backward traveling circumferential waves. In most of these works, the disk is assumed to be full. Chen and Jhu (1996) studied the in-plane vibration of spinning annular disks and investigated the effects of clamping ratio on the natural frequencies and stability of the disks. All these analyses demonstrate the existence of certain critical rotation speed at which one of the natural frequencies vanishes.

The in-plane stress distribution in a stationary annular disk under stationary edge tractions can be readily calculated by using the Airy stress function (Coker and Filon, 1957). On the other hand, the problem of a spinning disk under stationary edge loads has never been studied before. This problem is much more complex than the classical one with a nonrotating disk as a result of the Coriolis terms associated with the relative motion between the spinning disk and the stationary edge loads. In order to avoid the difficulties imposed by the Coriolis terms and the in-plane stresses due to centrifugal effect, Srinivasan and Ramamurti (1980) investigated a relevant problem of a stationary disk under a rotating concentrated edge load. Leung and Pinnington (1987) conducted experiments to measure the in-plane response of a stationary disk under rotating edge loads.

In the present paper we derive the analytical solutions for the in-plane stress and displacement distributions in a spinning disk under stationary edge tractions. The equations of in-plane vibration of the spinning disk with respect to the inertial frame are first derived. Lame's potentials are used to simplify the highly coupled equations. Numerical examples of stress and displacement distributions for a typical radius ratio are demonstrated. As the rotational speed of the disk approaches zero, the in-plane stresses and displacements are shown analytically to recover the solutions derived through the Airy stress function in the classical theory of linear elasticity.

Equations of Motion

Figure 1 shows an elastic annular disk spinning at constant speed Ω. The material of the disk is assumed to be homogeneous and isotropic with mass density ρ, Young's modulus E, and Poisson ratio ν. The spinning disk is clamped at inner radius $r = a$, and is subject to nonrotating edge tractions $\hat{\sigma}_{rr}$ and $\hat{\sigma}_{r\eta}$ at the outer radius $r = b$. (r, η) are the polar coordinates of a point on the spinning disk with respect to an inertial frame. If the disk is thin, plane stress conditions can be assumed and the equilibrium equations in the radial and tangential directions in terms of in-plane displacements u_r and u_θ can be written with respect to the body-fixed coordinate system (r, θ) (Burdess et al., 1987),

Contributed by the Applied Mechanics Division of THE AMERICAN SOCIETY OF MECHANICAL ENGINEERS for publication in the ASME JOURNAL OF APPLIED MECHANICS.

Discussion on the paper should be addressed to the Technical Editor, Professor Lewis T. Wheeler, Department of Mechanical Engineering, University of Houston, Houston, TX 77204-4792, and will be accepted until four months after final publication of the paper itself in the ASME JOURNAL OF APPLIED MECHANICS.

Manuscript received by the ASME Applied Mechanics Division, June 26, 1995; final revision, May 22, 1997. Associate Technical Editor: N. C. Perkins.

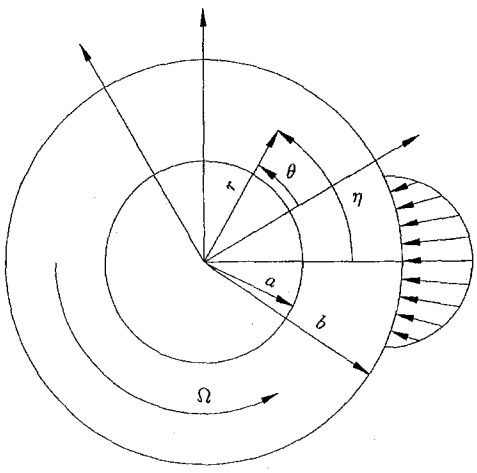

Fig. 1 A spinning annular disk under stationary edge load

$$\frac{E}{\rho(1-\nu^2)}(L_{11}u_r + L_{12}u_\theta) = \ddot{u}_r - 2\Omega\dot{u}_\theta - \Omega^2(u_r + r) \quad (1)$$

$$\frac{E}{\rho(1-\nu^2)}(L_{21}u_r + L_{22}u_\theta) = \ddot{u}_\theta + 2\Omega\dot{u}_r - \Omega^2 u_\theta \quad (2)$$

where the differential operators are defined as

$$L_{11} = \frac{\partial^2}{\partial r^2} + \frac{1}{r}\frac{\partial}{\partial r} - \frac{1}{r^2} + \frac{1-\nu}{2r^2}\frac{\partial^2}{\partial\theta^2} \quad (3)$$

$$L_{12} = \frac{1+\nu}{2}\frac{1}{r}\frac{\partial^2}{\partial r\partial\theta} - \frac{3-\nu}{2}\frac{1}{r^2}\frac{\partial}{\partial\theta} \quad (4)$$

$$L_{21} = \frac{1+\nu}{2}\frac{1}{r}\frac{\partial^2}{\partial r\partial\theta} + \frac{3-\nu}{2}\frac{1}{r^2}\frac{\partial}{\partial\theta} \quad (5)$$

$$L_{22} = \frac{1-\nu}{2}\left(\frac{\partial^2}{\partial r^2} + \frac{1}{r}\frac{\partial}{\partial r} - \frac{1}{r^2}\right) + \frac{1}{r^2}\frac{\partial^2}{\partial\theta^2}. \quad (6)$$

Equations (1) and (2) can be rewritten with respect to the inertial frame (r, η) by using the transformations

$$\dot{u}_r(r,\theta) = \frac{\partial u_r(r,\eta)}{\partial t} + \Omega\frac{\partial u_r(r,\eta)}{\partial\eta} \quad (7)$$

$$\dot{u}_\theta(r,\theta) = \frac{\partial u_\eta(r,\eta)}{\partial t} + \Omega\frac{\partial u_\eta(r,\eta)}{\partial\eta} \quad (8)$$

where

$$\eta = \theta + \Omega t. \quad (9)$$

It is convenient at this stage to introduce some dimensionless variables (denoted with an asterisk),

$$r^* = \frac{r}{b}, \quad \zeta = \frac{a}{b}, \quad u_r^* = \frac{u_r}{b}, \quad u_\eta^* = \frac{u_\eta}{b},$$

$$\Omega^* = \Omega b\sqrt{\frac{\rho}{E}}, \quad t^* = \frac{t}{b}\sqrt{\frac{E}{\rho}}$$

$$\sigma_{rr}^* = \frac{\sigma_{rr}}{E}, \quad \sigma_{r\eta}^* = \frac{\sigma_{r\eta}}{E}, \quad \sigma_{\eta\eta}^* = \frac{\sigma_{\eta\eta}}{E}$$

The equations of motion in terms of the dimensionless variables defined above with respect to the inertial frame can be written as follows:

$$\frac{1}{(1-\nu^2)}(L_{11}^* u_r^* + L_{12}^* u_\eta^*) = \left(\frac{\partial^2 u_r^*}{\partial t^{*2}} + 2\Omega^*\frac{\partial^2 u_r^*}{\partial t^*\partial\eta} + \Omega^{*2}\frac{\partial^2 u_r^*}{\partial\eta^2}\right) - 2\Omega^*\left(\frac{\partial u_\eta^*}{\partial t^*} + \Omega^*\frac{\partial u_\eta^*}{\partial\eta}\right) - \Omega^{*2}(u_r^* + r^*) \quad (10)$$

$$\frac{1}{(1-\nu^2)}(L_{21}^* u_r^* + L_{22}^* u_\eta^*) = \left(\frac{\partial^2 u_\eta^*}{\partial t^{*2}} + 2\Omega^*\frac{\partial^2 u_\eta^*}{\partial t^*\partial\eta} + \Omega^{*2}\frac{\partial^2 u_\eta^*}{\partial\eta^2}\right) + 2\Omega^*\left(\frac{\partial u_r^*}{\partial t^*} + \Omega^*\frac{\partial u_r^*}{\partial\eta}\right) - \Omega^{*2}u_\eta^*. \quad (11)$$

The differential operators L_{11}^*, L_{12}^*, L_{21}^*, and L_{22}^* are similar to those in Eqs. (3)–(6) with r and θ being replaced by r^* and η, respectively. The dimensionless boundary conditions with respect to the inertial frame are

$$u_r^* = u_\eta^* = 0 \quad \text{at } r^* = \zeta \quad (12a, b)$$

$$\frac{1}{1-\nu^2}\left[\frac{\partial u_r^*}{\partial r^*} + \nu\left(\frac{u_r^*}{r^*} + \frac{1}{r^*}\frac{\partial u_\eta^*}{\partial\eta}\right)\right] = \hat{\sigma}_{rr}^*(\eta)$$

$$\frac{1}{2(1+\nu)}\left(\frac{1}{r^*}\frac{\partial u_r^*}{\partial\eta} + \frac{\partial u_\eta^*}{\partial r^*} - \frac{u_\eta^*}{r^*}\right) = \hat{\sigma}_{r\eta}^*(\eta) \quad \text{at } r^* = 1. \quad (13a, b)$$

In the following discussion we drop all the asterisks for brevity.

It is noted that both the differential Eqs. (10) and (11), and the boundary conditions (12) and (13) are inhomogeneous. The superposition principle (Stakgold, 1979) permits us to decompose the problem into two simpler parts; one with inhomogeneous equations and homogeneous boundary conditions, and the other with homogeneous equations and inhomogeneous boundary conditions. The solution of the original problem can be obtained by reassembling these solutions of the simpler problems. For the first part, the forcing term $r\Omega^2$ in the inhomogeneous Eq. (10) is due to the centrifugal effect. When the steady-state solutions are concerned, this term is dominant compared to other contribution from the term $u_r\Omega^2$. Therefore, the solution of the first problem is the same as the classical problem of a freely spinning disk, and is well documented in the literature (Ono et al., 1991). On the other hand, the second problem has never been solved in the literature, and will be the subject of the following discussion.

Lame's Potentials

The homogeneous parts of Eqs. (10) and (11) can be simplified if Lame's potentials ϕ and ψ are introduced (Eringen and Suhubi, 1975):

$$u_r = \frac{\partial\phi}{\partial r} + \frac{1}{r}\frac{\partial\psi}{\partial\eta} \quad (14)$$

$$u_\eta = \frac{1}{r}\frac{\partial\phi}{\partial\eta} - \frac{\partial\psi}{\partial r}. \quad (15)$$

As a consequence, the stress components can also be represented as

$$\sigma_{rr} = \frac{\nu}{1-\nu^2}\nabla^2\phi + \frac{1}{1+\nu}\left(\frac{\partial^2\phi}{\partial r^2} - \frac{1}{r^2}\frac{\partial\psi}{\partial\eta} + \frac{1}{r}\frac{\partial^2\psi}{\partial r\partial\eta}\right) \quad (16)$$

$$\sigma_{r\eta} = \frac{1}{2(1+\nu)}\left(\frac{2}{r}\frac{\partial^2\phi}{\partial r\partial\eta} - \frac{2}{r^2}\frac{\partial\phi}{\partial\eta} - \frac{\partial^2\psi}{\partial r^2} + \frac{1}{r}\frac{\partial\psi}{\partial r} + \frac{1}{r^2}\frac{\partial^2\psi}{\partial\eta^2}\right) \quad (17)$$

$$\sigma_{\eta\eta} = \frac{\nu}{1-\nu^2}\nabla^2\phi + \frac{1}{1+\nu}\left(\frac{1}{r}\frac{\partial\phi}{\partial r} + \frac{1}{r^2}\frac{\partial^2\phi}{\partial\eta^2} + \frac{1}{r^2}\frac{\partial\psi}{\partial\eta} - \frac{1}{r}\frac{\partial^2\psi}{\partial r\partial\eta}\right). \quad (18)$$

It is assumed that the edge traction is applied for a long time and the steady state prevails as seen by an observer in the inertial frame. Substituting Eqs. (14) and (15) into homogeneous parts of Eqs. (10) and (11) and neglecting all the temporal derivatives result in the following equations:

$$\frac{\partial G}{\partial r} + \frac{1}{r}\frac{\partial H}{\partial\eta} = 0 \quad (19)$$

$$\frac{1}{r}\frac{\partial G}{\partial\eta} - \frac{\partial H}{\partial r} = 0 \quad (20)$$

where

$$G = \lambda_1^2\nabla^2\phi - \Omega^2\frac{\partial^2\phi}{\partial\eta^2} + \Omega^2\phi - 2\Omega^2\frac{\partial\psi}{\partial\eta} \quad (21)$$

$$H = \lambda_2^2\nabla^2\psi - \Omega^2\frac{\partial^2\psi}{\partial\eta^2} + \Omega^2\psi + 2\Omega^2\frac{\partial\phi}{\partial\eta}. \quad (22)$$

λ_1 and λ_2 are two constants depending on the Poisson ratio,

$$\lambda_1^2 = \frac{1}{1-\nu^2}, \quad \lambda_2^2 = \frac{1}{2(1+\nu)}. \quad (23a, b)$$

It is noted that for the problem of a fixed disk described by an observer rotating with speed Ω, Eqs. (21) and (22) should read (Srinivasan and Ramamurti, 1980)

$$G = \lambda_1^2\nabla^2\phi - \Omega^2\frac{\partial^2\phi}{\partial\eta^2},$$

$$H = \lambda_2^2\nabla^2\psi - \Omega^2\frac{\partial^2\psi}{\partial\eta^2}. \quad (24a, b)$$

As a consequence, the problem of a stationary disk under rotating edge loads differs from the problem of a rotating disk under stationary edge loads not only by the centrifugal effect, but also by additional terms arising from Coriolis effect. It is noted that for the problem of a stationary disk under rotating edge loads, the equilibrium equations are decoupled into equations for ϕ and ψ, respectively, and have been investigated by Srinivasan and Ramamurti (1980).

The general solutions for G and H in Eqs. (19) and (20) can be expressed in the form

$$G = A_0 + \sum_{n=1}^{\infty}\left[(A_n r^n + B_n r^{-n})\cos n\eta + (A_n' r^n + B_n' r^{-n})\sin n\eta\right] \quad (25)$$

$$H = A_0' + \sum_{n=1}^{\infty}\left[(A_n' r^n - B_n' r^{-n})\cos n\eta + (-A_n r^n + B_n r^{-n})\sin n\eta\right] \quad (26)$$

where A_n, B_n, A_n', and B_n' are undetermined constants. Equations (21) and (22) are two inhomogeneous equations for ϕ and ψ. Since the corresponding solutions must be periodic in η, the solutions for ϕ and ψ can be expressed in Fourier series as

$$\phi(r,\eta) = \Phi_{0c} + \sum_{n=1}^{\infty}\Phi_{nc}(r)\cos n\eta + \Phi_{ns}(r)\sin n\eta \quad (27)$$

$$\psi(r,\eta) = \Psi_{0c} + \sum_{n=1}^{\infty}\Psi_{nc}(r)\cos n\eta + \Psi_{ns}(r)\sin n\eta. \quad (28)$$

Since the Fourier components are orthogonal, the solutions can be treated separately for different Fourier component.

Case $n = 0$: This case corresponds to the spinning disk under uniform traction. Φ_{0c} and Ψ_{0c} can be solved as

$$\Phi_{0c} = c_0 J_0(\beta_{01}r) + e_0 Y_0(\beta_{01}r) + A_0\frac{1}{\Omega^2} \quad (29)$$

$$\Psi_{0c} = -d_0' J_0(\beta_{02}r) - f_0' Y_0(\beta_{02}r) + A_0'\frac{1}{\Omega^2} \quad (30)$$

where J and Y are Bessel functions of the first and the second kinds, respectively. β_{01} and β_{02} are defined as

$$\beta_{01} = \frac{\Omega}{\lambda_1} \quad \text{and} \quad \beta_{02} = \frac{\Omega}{\lambda_2}. \quad (31)$$

Constants A_0 and A_0' do not affect the displacement and the stress fields in the spinning disk and can be ignored.

Case $n \geq 2$: The general solutions for this case are

$$\Phi_{nc} = c_n J_n(\beta_{n1}r) + d_n s_{n1} J_n(\beta_{n2}r) + e_n Y_n(\beta_{n1}r) + f_n s_{n1} Y_n(\beta_{n2}r) + \frac{A_n r^n}{(1+n)^2\Omega^2} + \frac{B_n r^{-n}}{(1-n)^2\Omega^2} \quad (32)$$

$$\Psi_{ns} = c_n s_{n2} J_n(\beta_{n1}r) + d_n J_n(\beta_{n2}r) + e_n s_{n2} Y_n(\beta_{n1}r) + f_n Y_n(\beta_{n2}r) - \frac{A_n r^n}{(1+n)^2\Omega^2} + \frac{B_n r^{-n}}{(1-n)^2\Omega^2} \quad (33)$$

$$\Phi_{ns} = c_n' J_n(\beta_{n1}r) + d_n' s_{n1} J_n(\beta_{n2}r) + e_n' Y_n(\beta_{n1}r) + f_n' s_{n1} Y_n(\beta_{n2}r) + \frac{A_n' r^n}{(1+n)^2\Omega^2} + \frac{B_n' r^{-n}}{(1-n)^2\Omega^2} \quad (34)$$

$$\Psi_{nc} = -c_n' s_{n2} J_n(\beta_{n1}r) - d_n' J_n(\beta_{n2}r) - e_n' s_{n2} Y_n(\beta_{n1}r) - f_n' Y_n(\beta_{n2}r) + \frac{A_n' r^n}{(1+n)^2\Omega^2} - \frac{B_n' r^{-n}}{(1-n)^2\Omega^2}. \quad (35)$$

β_{n1} and β_{n2} are positive real roots of the following quartic equation:

$$\lambda_1^2\lambda_2^2\beta^4 - (\lambda_1^2 + \lambda_2^2)(1+n^2)\Omega^2\beta^2 + (1-n^2)^2\Omega^4 = 0. \quad (36)$$

s_{n1} and s_{n2} are defined as

$$s_{n1} = \frac{2n\Omega^2}{(1+n^2)\Omega^2 - \lambda_1^2\beta_{n2}^2} \quad \text{and}$$

$$s_{n2} = \frac{2n\Omega^2}{(1+n^2)\Omega^2 - \lambda_2^2\beta_{n1}^2}. \quad (37a, b)$$

It is noted that constants s_{n1} and s_{n2} are independent of Ω because β_{n1} and β_{n2} are proportional to Ω. Again, the terms associated with constants A_n, A_n', B_n, B_n' will not affect the stress and displacement fields of the loaded disk and can be ignored.

Case $n = 1$: The solution for this case can not be generalized from the case $n \geq 2$, because one of the two β's vanishes. The general solution for this case can be found as

$$\Phi_{1c} = d_1 s_{11} J_1(\beta_{12} r) + f_1 s_{11} Y_1(\beta_{12} r) + A_1 \frac{r}{2\Omega^2} + B_1 \frac{r \ln r}{\lambda_1^2 + \lambda_2^2} + \chi_1 r + \chi_2 \frac{1}{r} \quad (38)$$

$$\Psi_{1s} = d_1 J_1(\beta_{12} r) + f_1 Y_1(\beta_{12} r) + B_1 \frac{1}{\lambda_1^2 + \lambda_2^2} \left(r \ln r + \frac{\lambda_1^2 - \lambda_2^2}{2r\Omega^2} \right) + \chi_1 r + \chi_2 \frac{1}{r} \quad (39)$$

$$\Phi_{1s} = d_1' s_{11} J_1(\beta_{12} r) + f_1' s_{11} Y_1(\beta_{12} r) + A_1' \frac{r}{2\Omega^2} + B_1' \frac{r \ln r}{\lambda_1^2 + \lambda_2^2} + \chi_1' r + \chi_2' \frac{1}{r} \quad (40)$$

$$\Psi_{1c} = -d_1' J_1(\beta_{12} r) - f_1' Y_1(\beta_{12} r) - B_1' \frac{1}{\lambda_1^2 + \lambda_2^2} \left(r \ln r + \frac{\lambda_1^2 - \lambda_2^2}{2r\Omega^2} \right) - \chi_1' r - \chi_2' \frac{1}{r}. \quad (41)$$

β_{12} from Eq. (36) and s_{11} from Eq. (37a) are found to be

$$\beta_{12} = \frac{\sqrt{3 - \nu}}{\lambda_2} \Omega \quad \text{and} \quad s_{11} = -\frac{1 - \nu}{2}.$$

Unlike the cases for $n \neq 1$, the terms associated with constants A_1, B_1, A_1', and B_1' contribute to the stress and displacement fields of the spinning disk. On the other hand, the homogeneous solutions associated with constants χ_1, χ_2, χ_1', and χ_2' are irrelevant to the stress and displacement fields, and can be ignored.

Stress and Displacement Fields

After obtaining the solutions for ϕ and ψ we can write the general expressions of the in-plane stress and displacement fields for a spinning disk under stationary edge loads. It is assumed that the edge load on the outer boundary can be expanded in the following Fourier series:

$$\hat{\sigma}_{rr}(\eta) = \sum_{n=0}^{\infty} p_n \cos n\eta + p_n' \sin n\eta \quad (42)$$

$$\hat{\sigma}_{r\eta}(\eta) = \sum_{n=0}^{\infty} q_n' \cos n\eta + q_n \sin n\eta. \quad (43)$$

The above traction boundary conditions can be divided into two parts. The first part involves only symmetric $\hat{\sigma}_{rr}(\eta)$ and antisymmetric $\hat{\sigma}_{r\eta}(\eta)$ (i.e., $p_n' = q_n' = 0$ in Eqs. (42), (43)), and the second part involves only antisymmetric $\hat{\sigma}_{rr}(\eta)$ and symmetric $\hat{\sigma}_{r\eta}(\eta)$. The complete solution may be obtained by reassembling these two solutions. For the first problem with $p_n' = q_n' = 0$, the stress and displacement fields of the loaded disk are

$$(1 - \nu^2)\sigma_{rr}(r, \eta) = B_1(2\mu_1 r^{-1} - \mu_2 r^{-3}) \cos \eta + \sum_{n=0}^{\infty} \cos n\eta \{ c_n[(\kappa_{n1} r^{-2} - \beta_{n1}^2) J_n(\beta_{n1} r) + \kappa_{n2} r^{-1} J_{n+1}(\beta_{n1} r)] + d_n[(\kappa_{n3} r^{-2} - s_{n1}\beta_{n2}^2) J_n(\beta_{n2} r) + \kappa_{n4} r^{-1} J_{n+1}(\beta_{n2} r)] + e_n[(\kappa_{n1} r^{-2} - \beta_{n1}^2) Y_n(\beta_{n1} r) + \kappa_{n2} r^{-1} Y_{n+1}(\beta_{n1} r)] + f_n[(\kappa_{n3} r^{-2} - s_{n1}\beta_{n2}^2) Y_n(\beta_{n2} r) + \kappa_{n4} r^{-1} Y_{n+1}(\beta_{n2} r)] \} \quad (44)$$

$$(1 - \nu^2)\sigma_{r\eta}(r, \eta) = -B_1(\mu_0\mu_1 r^{-1} + \mu_2 r^{-3}) \sin \eta + \sum_{n=0}^{\infty} \sin n\eta [c_n \{ (\tfrac{1}{2}\mu_0 s_{n2}\beta_{n1}^2 - \kappa_{n1} r^{-2}) J_n(\beta_{n1} r) - \kappa_{n5} r^{-1} J_{n+1}(\beta_{n1} r) \} + d_n[(\tfrac{1}{2}\mu_0\beta_{n2}^2 - \kappa_{n3} r^{-2}) J_n(\beta_{n2} r) - \kappa_{n6} r^{-1} J_{n+1}(\beta_{n2} r)] + e_n \{ (\tfrac{1}{2}\mu_0 s_{n2}\beta_{n1}^2 - \kappa_{n1} r^{-2}) Y_n(\beta_{n1} r) - \kappa_{n5}\beta_{n1} r^{-1} Y_{n+1}(\beta_{n1} r) \} + f_n[(\tfrac{1}{2}\mu_0\beta_{n2}^2 - \kappa_{n3} r^{-2}) Y_n(\beta_{n2} r) - \kappa_{n6} r^{-1} Y_{n+1}(\beta_{n2} r)] \} \quad (45)$$

$$(1 - \nu^2)\sigma_{\eta\eta}(r, \eta) = B_1(2\nu\mu_1 r^{-1} + \mu_2 r^{-3}) \cos \eta + \sum_{n=0}^{\infty} \cos n\eta \{ c_n[(-\kappa_{n1} r^{-2} - \nu\beta_{n1}^2) J_n(\beta_{n1} r) - \kappa_{n2} r^{-1} J_{n+1}(\beta_{n1} r)] + d_n[(-\kappa_{n3} r^{-2} - \nu s_{n1}\beta_{n2}^2) J_n(\beta_{n2} r) - \kappa_{n4} r^{-1} J_{n+1}(\beta_{n2} r)] + e_n[(-\kappa_{n1} r^{-2} - \nu\beta_{n1}^2) Y_n(\beta_{n1} r) - \kappa_{n2} r^{-1} Y_{n+1}(\beta_{n1} r)] \} + f_n[(-\kappa_{n3} r^{-2} - \nu s_{n1}\beta_{n2}^2) Y_n(\beta_{n2} r) - \kappa_{n4} r^{-1} Y_{n+1}(\beta_{n2} r)] \} \quad (46)$$

$$u_r(r, \eta) = \cos \eta \left\{ \frac{A_1}{2\Omega^2} + B_1 \left[\mu_1(1 + 2 \ln r) + \frac{1}{2} \frac{\mu_2}{\mu_0} r^{-2} \right] \right\} + \sum_{n=0}^{\infty} \cos n\eta \{ c_n[\kappa_{n8} r^{-1} J_n(\beta_{n1} r) - \beta_{n1} J_{n+1}(\beta_{n1} r)] + d_n[\kappa_{n7} r^{-1} J_n(\beta_{n2} r) - s_{n1}\beta_{n2} J_{n+1}(\beta_{n2} r)] + e_n[\kappa_{n8} r^{-1} Y_n(\beta_{n1} r) - \beta_{n1} Y_{n+1}(\beta_{n1} r)] + f_n[\kappa_{n7} r^{-1} Y_n(\beta_{n2} r) - s_{n1}\beta_{n2} Y_{n+1}(\beta_{n2} r)] \} \quad (47)$$

$$u_\eta(r, \eta) = -\sin \eta \left\{ \frac{A_1}{2\Omega^2} + B_1 \left[\mu_1(1 + 2 \ln r) - \frac{1}{2} \frac{\mu_2}{\mu_0} r^{-2} \right] \right\} + \sum_{n=0}^{\infty} \sin n\eta \{ c_n[s_{n2}\beta_{n1} J_{n+1}(\beta_{n1} r) - \kappa_{n8} r^{-1} J_n(\beta_{n1} r)] + d_n[\beta_{n2} J_{n+1}(\beta_{n2} r) - \kappa_{n7} r^{-1} J_n(\beta_{n2} r)] + e_n[s_{n2}\beta_{n1} Y_{n+1}(\beta_{n1} r) - \kappa_{n8} r^{-1} Y_n(\beta_{n1} r)] + f_n[\beta_{n2} Y_{n+1}(\beta_{n2} r) - \kappa_{n7} r^{-1} Y_n(\beta_{n2} r)] \} \quad (48)$$

where the constants μ's and κ's are defined as follows:

$$\mu_0 = 1 - \nu, \quad \mu_1 = (\lambda_1^2 + \lambda_2^2)^{-1}, \quad \mu_2 = \mu_0\mu_1(\lambda_1^2 - \lambda_2^2)\Omega^{-2}$$

$$\kappa_{n1} = \mu_0(1 + s_{n2})(n^2 - n), \quad \kappa_{n2} = \mu_0(1 - n s_{n2})\beta_{n1},$$

$$\kappa_{n3} = \mu_0(1 + s_{n1})(n^2 - n), \quad \kappa_{n4} = -\mu_0(n - s_{n1})\beta_{n2},$$

$$\kappa_{n5} = -\mu_0(n - s_{n2})\beta_{n1}, \quad \kappa_{n6} = \mu_0(1 - n s_{n1})\beta_{n2},$$

$$\kappa_{n7} = n(1 + s_{n1}), \quad \kappa_{n8} = n(1 + s_{n2}).$$

The terms containing constants d_0, f_0, c_1, and e_1, which have not been defined before, in Eqs. (44)–(48) should be ignored. Their presence in Eqs. (44)–(48) is solely to make the equations more compact. Equations (44)–(48) are in analogy with the classical solutions derived through the Airy stress function for a stationary annular disk under stationary edge loads (Coker and Filon, 1957). From boundary conditions (42) and (43), together with the zero displacement conditions (12) on the inner radius, one can determine the constants in Eqs. (44)–(48) uniquely.

When the traction boundary conditions involve only antisymmetric $\hat{\sigma}_{rr}(\eta)$ and symmetric $\hat{\sigma}_{r\eta}(\eta)$, i.e., $p_n = q_n = 0$, the equations for stress and displacement can be obtained from Eqs. (44)–(48) by replacing c_n, e_n, d_n, f_n, A_1, and B_1 with their primed counterparts, bearing in mind that the terms containing

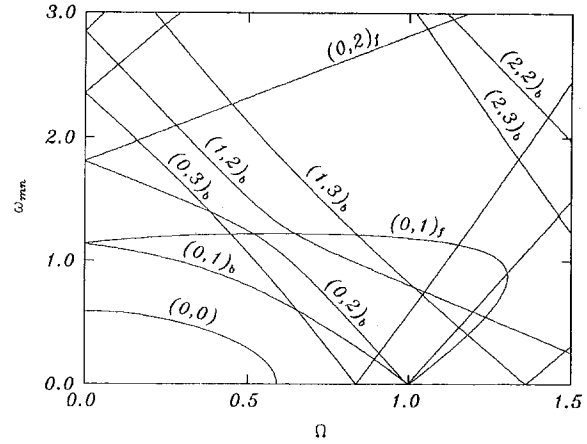

Fig. 2 Natural frequencies of in-plane vibration for a freely spinning disk with radius ratio 0.3

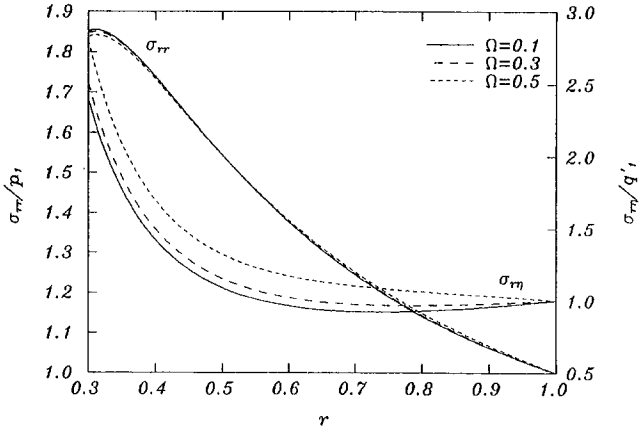

Fig. 4 The curves denoted σ_{rr} represent normal stress distribution for a disk under normal edge traction $\hat{\sigma}_{rr} = p_1 \cos \eta$. The curves denoted $\sigma_{r\eta}$ represent shear stress distribution for a disk under shear edge traction $\hat{\sigma}_{r\eta} = q'_1 \cos \eta$.

constants c'_0, e'_0, c'_1, and e'_1 should be ignored. In the meantime cos $n\eta$ in Eqs. (44), (46), (47) should be replaced by sin $n\eta$, while sin $n\eta$ in Eqs. (45), (48) should be replaced by $-\cos n\eta$.

Numerical Examples

Before presenting the stress and displacement distributions, we first examine the natural frequencies of the in-plane vibration of the freely spinning disk (Chen and Jhu, 1996). Figure 2 shows the relation between dimensionless natural frequency ω_{mn} and dimensionless rotational speed Ω for radius ratio $\zeta = 0.3$. For simplicity, only the modes with less than four nodal diameters are shown in Fig. 2. The definition of ω_{mn} is the same as that of Ω, i.e., multiplying the physical natural frequency by $b\sqrt{\rho/E}$. The Poisson ratio is assumed to be 0.3. The mode label $(m, n)_f$ represents the forward traveling modes with m nodal circles and n nodal diameters. Similarly, the subscript "b" represents a backward traveling wave. The critical speed Ω_{cn} is defined as the rotational speed at which the natural frequency of the mode $(0, n)_b$ vanishes. The first critical speed in Fig. 2 is $\Omega_{c0} = 0.591$ corresponding to the mode (0, 0). Beyond this critical speed the natural frequency ω_{00} becomes purely imaginary, and divergence instability is induced. The critical speeds corresponding to the modes with $n = 1, 2, 3$ are 0.998, 0.995, and 0.836, respectively. It is noted that mode (0, 0) is a torsional mode which involves displacement u_η only, while mode (1, 0) (beyond the range of Fig. 2) is a radial mode which involves displacement u_r only (Chen and Jhu, 1996). All the modes with nodal diameters involve both torsional and radial vibrations at the same time.

The curves denoted σ_{rr} in Figs. 3 to 5 represent the normal stress distributions along the radius from inner to outer boundary for a disk under normal edge tractions $\hat{\sigma}_{rr}(\eta) = p_n \cos n\eta$, where $n = 0$, 1, and 2, respectively, for three rotational speeds ($\Omega = 0.1$, 0.3, 0.5). On the other hand, the curves denoted $\sigma_{r\eta}$ in Figs. 3 to 5 represent the shear stress distributions for a disk under tangential edge tractions $\hat{\sigma}_{r\eta}(\eta) = q'_n \cos n\eta$. The scales for σ_{rr} and $\sigma_{r\eta}$ are different, as shown in these figures. In general, the amplitude of the stress field increases significantly as Ω increases. However, Figs. 3 and 4 show that the stress field is much more susceptible to tangential edge traction than to normal edge traction in the cases of $n = 0$ and 1.

It is noted that numerical difficulties arise in solving the constants in Eqs. (44) – (48) as the rotational speed approaches zero. More specifically, the constants c_n, d_n approach infinite and e_n, f_n approach zero as Ω approaches zero. In order to compare the above results with the case of a nonrotating disk, we obtain the solutions for $\Omega = 0$ separately through the use of the Airy stress function in the classical theory of linear elasticity. We find that the curves for $\Omega = 0$ are indistinguishable from the curves for $\Omega = 0.1$ in Figs. 3 through 5.

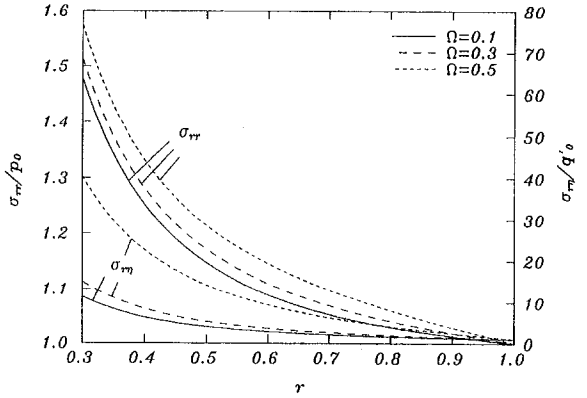

Fig. 3 The curves denoted σ_{rr} represent normal stress distribution along the radius for a disk under uniform normal edge traction $\hat{\sigma}_{rr} = p_0$. The curves denoted $\sigma_{r\eta}$ represent shear stress distribution for a disk under shear edge traction $\hat{\sigma}_{r\eta} = q'_0$.

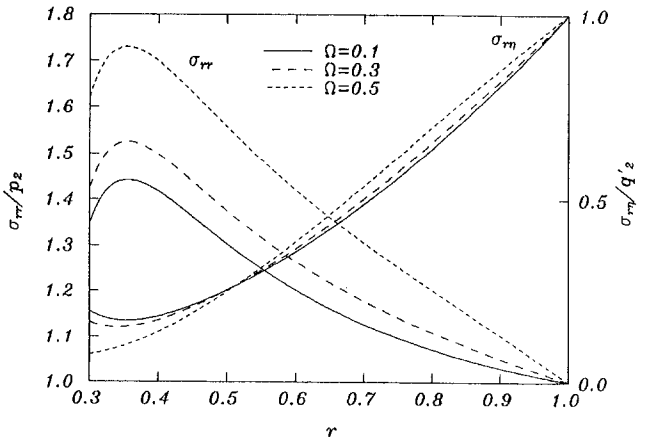

Fig. 5 The curves denoted σ_{rr} represent normal stress distribution for a disk under normal edge traction $\hat{\sigma}_{rr} = p_2 \cos 2\eta$. The curves denoted $\sigma_{r\eta}$ represent shear stress distribution for a disk under shear edge traction $\hat{\sigma}_{r\eta} = q'_2 \cos 2\eta$.

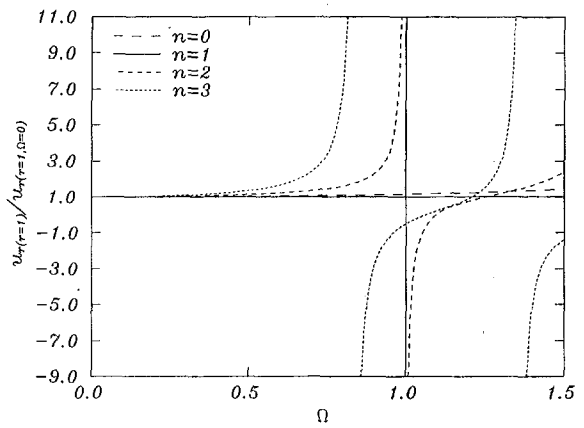

Fig. 6 Effect of rotational speed Ω on the displacement at the outer radius for a spinning disk under normal edge traction $\hat{\sigma}_{rr} = p_n \cos n\eta$

Figure 6 shows the displacement ratio $u_r/u_{r(\Omega=0)}$ at point ($r = 1$, $\eta = 0$) as function of Ω when the spinning disk is under normal edge traction $\hat{\sigma}_{rr}(\eta) = p_n \cos n\eta$. Similarly, Fig. 7 shows the relation between $u_\eta/u_{\eta(\Omega=0)}$ and Ω when the disk is under tangential edge traction $\hat{\sigma}_{r\eta}(\eta) = q_n' \cos n\eta$. For the case when the disk is under uniform normal edge traction ($n = 0$), the steady-state displacement is rather small even when the disk is spinning beyond the critical speed, as shown in Fig. 6. On the other hand, when the disk is under uniform tangential traction, the displacement grows unboundedly as Ω approaches Ω_{c0}. Steady-state response does not exist when the disk is spinning beyond the critical speed and under uniform tangential traction. This phenomenon reflects the fact that mode (0, 0) is of torsional nature. For the case when $n \geq 1$, on the other hand, either normal or tangential edge load tends to induce unbounded displacement as long as Ω is close to Ω_{cn}. It is noted in Fig. 6 that while u_r jumps to $\pm\infty$ as Ω approaches Ω_{c1}, the radial displacement is rather insentive to the rotation speed when Ω is away from Ω_{c1}.

Special Case as Ω Approaches Zero

From the above numerical calculations, we observe that the stress and displacement distributions for a spinning disk under stationary edge loads recover the classical solutions of a stationary disk under stationary edge loads as Ω approaches zero. In this section we show in an analytical manner that formulae (44)–(48) can indeed recover the classical formulae derived through the Airy stress function. Since numerical experience shows that constants c_n and d_n approach infinite, while e_n and f_n approach zero as Ω approaches zero, additional analyses are needed in this limit case.

Case $n = 0$: When the rotational speed Ω approaches zero, Bessel functions $J_0(x)$ and $Y_0(x)$ can be approximated by $1 - x^2/4$ and $2 \ln x/\pi$, respectively. Consequently, the nontrivial solutions for Φ_{0c} and Ψ_{0c} can be reduced to

$$\Phi_{0c} = \hat{c}_0 r^2 + \hat{e}_0 \ln r \tag{49}$$

$$\Psi_{0c} = \hat{d}_0' r^2 + \hat{f}_0' \ln r \tag{50}$$

where

$$\hat{c}_0 = -\frac{\Omega^2}{4\lambda_1^2} c_0, \quad \hat{e}_0 = \frac{2}{\pi} e_0, \quad \hat{d}_0' = \frac{\Omega^2}{4\lambda_2^2} d_0', \quad \hat{f}_0' = -\frac{2}{\pi} f_0'.$$

The stress and displacement fields deduced from Eqs. (49) and (50) recover the classical solutions deduced from the Airy stress function.

Case $n \geq 2$: In this case Bessel functions $J_n(x)$ and $Y_n(x)$ can be approximated as

$$J_n(x) \approx \frac{x^n}{2^n n!} - \frac{x^{n+2}}{2^{n+2}(n+1)!} \tag{51}$$

$$Y_n(x) \approx \frac{2^n (n-1)!}{-\pi x^n} + \frac{2^{n-2}(n-2)!}{-\pi x^{n-2}}. \tag{52}$$

For the problem with $p_n' = q_n' = 0$, the matrix equation for determining constants c_n, d_n, e_n, f_n can be reduced to

$$\begin{bmatrix} g_{11} + \beta_{n1}^2 h_{11} & g_{12} + \beta_{n2}^2 h_{12} & g_{13} + \beta_{n1}^2 h_{13} & g_{14} + \beta_{n2}^2 h_{14} \\ g_{21} + \beta_{n1}^2 h_{21} & g_{22} + \beta_{n2}^2 h_{22} & g_{23} + \beta_{n1}^2 h_{23} & g_{24} + \beta_{n2}^2 h_{24} \\ g_{31} + \beta_{n1}^2 h_{31} & g_{32} + \beta_{n2}^2 h_{32} & g_{33} + \beta_{n1}^2 h_{33} & g_{34} + \beta_{n2}^2 h_{34} \\ g_{41} + \beta_{n1}^2 h_{41} & g_{42} + \beta_{n2}^2 h_{42} & g_{43} + \beta_{n1}^2 h_{43} & g_{44} + \beta_{n2}^2 h_{44} \end{bmatrix} \times \begin{Bmatrix} \hat{c}_n \\ \hat{d}_n \\ \hat{e}_n \\ \hat{f}_n \end{Bmatrix} = \begin{Bmatrix} 0 \\ 0 \\ p_n \\ q_n \end{Bmatrix} \tag{53}$$

where $\hat{c}_n$, $\hat{d}_n$, $\hat{e}_n$, $\hat{f}_n$ are defined as

$$\hat{c}_n = \frac{\beta_{n1}^n c_n}{2^n n!}, \quad \hat{d}_n = \frac{\beta_{n2}^n d_n}{2^n n!}, \quad \hat{e}_n = \frac{2^n n! e_n}{\pi \beta_{n1}^n}, \quad \hat{f}_n = \frac{2^n n! f_n}{\pi \beta_{n2}^n}.$$

The constants g_{ij} and h_{ij} are given in Appendix. Since β_{n1} and β_{n2} are proportional to Ω, the terms containing constants h_{ij} are relatively unimportant in comparing with the terms containing constants g_{ij}. However, the terms containing h_{ij} should not be left out of matrix Eq. (53) entirely because the determinant of matrix g_{ij} vanishes. If we subtract the first row of Eq. (53) by the second row, and subtract the third row by the fourth row, we obtain two equations

$$[2g_{11} r^{n-1} + O(\beta_{n1}^2)]\hat{c}_n + [2g_{12} r^{n-1} + O(\beta_{n1}^2)]\hat{d}_n + O(\beta_{n1}^2)\hat{e}_n + O(\beta_{n1}^2)\hat{f}_n = 0 \tag{54}$$

$$[2g_{31} r^{n-1} + O(\beta_{n1}^2)]\hat{c}_n + [2g_{32} r^{n-1} + O(\beta_{n1}^2)]\hat{d}_n + O(\beta_{n1}^2)\hat{e}_n + O(\beta_{n1}^2)\hat{f}_n = p_n - q_n. \tag{55}$$

$O(\beta_{n1}^2)$ represents the terms proportional to β_{n1}^2, and are relatively small as Ω approaches zero. Therefore, as Ω approaches zero the terms containing $\hat{e}_n$ and $\hat{f}_n$ can be neglected in Eqs. (54) and (55). Since determinant $\begin{vmatrix} g_{11} & g_{12} \\ g_{31} & g_{32} \end{vmatrix} = 0$, the ratio between $\hat{c}_n$ and $\hat{d}_n$ approaches a constant value, i.e.,

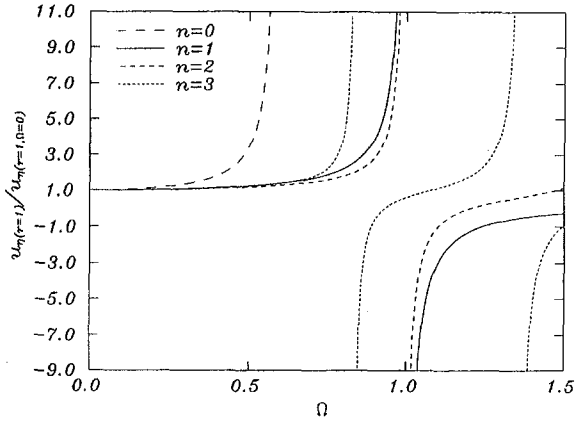

Fig. 7 Effect of rotational speed Ω on the displacement at the outer radius for a spinning disk under tangential edge traction $\hat{\sigma}_{r\eta} = q_n' \cos n\eta$

$$\frac{\hat{c}_n}{\hat{d}_n} = -\frac{g_{12}}{g_{11}} = \frac{(1-\nu-2s_{n1})\beta_{n2}^2}{(2-s_{n2}+\nu s_{n2})\beta_{n1}^2}, \tag{56}$$

while the constants $\hat{c}_n$ and $\hat{d}_n$ approach infinite as Ω approaches zero. It is noted that while the values of $\hat{c}_n$ and $\hat{d}_n$ depend on the boundary conditions p_n and q_n, the ratio in Eq. (56) is independent of the boundary conditions. This fact has also been verified numerically. By a similar procedure, with adding rows instead of subtracting, we conclude that the ratio between $\hat{e}_n$ and $\hat{f}_n$ approaches a constant value,

$$\frac{\hat{e}_n}{\hat{f}_n} = -\frac{g_{14}}{g_{13}} = \frac{(-1+\nu-2s_{n1})\beta_{n2}^2}{(2+s_{n2}-\nu s_{n2})\beta_{n1}^2}. \tag{57}$$

With the observations from Eqs. (56), (57), and the approximations (51), (52), the classical solutions for a stationary annular disk under stationary in-plane edge load can be recovered from solutions (44)–(48).

Case $n = 1$: In this case Bessel function $J_1(x)$ can be obtained from Eq. (51), while $Y_1(x)$ can be approximated as

$$Y_1(x) \approx \frac{x \ln x}{\pi} - \frac{(\ln 2 - \gamma)x}{\pi} - \frac{2}{\pi x} - \frac{x}{2\pi}$$

where γ denotes Euler's constant defined by

$$\gamma = \lim_{n\to\infty}\left(1 + \frac{1}{2} + \frac{1}{3} + \ldots + \frac{1}{n} - \ln n\right) = 0.5772\ldots.$$

As Ω approaches zero, the matrix equation for determining constants d_1, f_1, A_1, and B_1 can be reduced to

$$\begin{bmatrix} t_{11}+\beta_{12}^2 w_{11} & t_{12}+\beta_{12}^2 w_{12} & 1 & t_{14}+\Omega^2 w_{14} \\ t_{21}+\beta_{12}^2 w_{21} & t_{22}+\beta_{12}^2 w_{22} & -1 & t_{24}+\Omega^2 w_{24} \\ \beta_{12}^2 w_{31} & t_{32}+\beta_{12}^2 w_{32} & 0 & t_{34}+\Omega^2 w_{34} \\ \beta_{12}^2 w_{41} & t_{42}+\beta_{12}^2 w_{42} & 0 & t_{44}+\Omega^2 w_{44} \end{bmatrix} \times \begin{Bmatrix} \hat{d}_1 \\ \hat{f}_1 \\ \hat{A}_1 \\ \hat{B}_1 \end{Bmatrix} = \begin{Bmatrix} 0 \\ 0 \\ p_1 \\ q_1 \end{Bmatrix} \tag{58}$$

where $\hat{d}_1, \hat{f}_1, \hat{A}_1$, and $\hat{B}_1$ are defined as

$$\hat{d}_1 = \frac{\beta_{12}}{2} d_1, \quad \hat{f}_1 = \frac{2}{\pi\beta_{12}} f_1, \quad \hat{A}_1 = \frac{1}{2\Omega^2} A_1, \quad \hat{B}_1 = \frac{1}{\Omega^2} B_1.$$

t_{ij} and w_{ij} are defined in the Appendix. After adding the first two rows, and adding the last two rows of Eq. (58), one obtains

$$O(\beta_{12}^2)\hat{d}_1 + [2t_{12} + O(\beta_{12}^2)]\hat{f}_1 + [2t_{14} + O(\Omega^2)]\hat{B}_1 = 0 \tag{59}$$

$$O(\beta_{12}^2)\hat{d}_1 + [2t_{32} + O(\beta_{12}^2)]\hat{f}_1 + [2t_{34} + O(\Omega^2)]\hat{B}_1 = p_1 + q_1 \tag{60}$$

By following the similar argument as that used in the previous case for $n \geq 2$, we can conclude that the ratio between $\hat{f}_1$ and $\hat{B}_1$ approaches a constant value

$$\frac{\hat{f}_1}{\hat{B}_1} = -\frac{t_{14}}{t_{12}} = \frac{2(1+\nu)^2\Omega^2}{(3-\nu)\beta_{12}^2}. \tag{61}$$

With the observation from Eq. (61), the classical solutions for a stationary annular disk under stationary in-plane edge load can be recovered from Eqs. (44)–(48).

Conclusions and Discussions

The steady-state in-plane response of a spinning annular disk under stationary edge traction is investigated analytically. The results of this study can be summarized as follows.

1 The problem of a spinning disk-stationary load differs from the problem of a stationary disk-spinning load not only by the centrifugal effect, but also by the terms arising from the Coriolis effect.

2 While the equilibrium equations for the stationary disk-spinning load system can be decoupled by using Lame's potentials, the equations for the spinning disk-stationary load system cannot be completely decoupled. This renders the problem of a spinning disk-stationary load much more complicated.

3 The general solutions for the steady-state stress and displacement distributions are derived explicitly in the series form. These formulae are in analogy with the solutions for a stationary disk under stationary edge load, which are derived through the use of the Airy stress function in the classical theory of linear elasticity.

4 When the spinning disk is under uniform normal edge traction, the displacement response is rather small even when the rotational speed Ω is beyond the critical speed Ω_{c0}. When the disk is under uniform tangential edge traction, on the other hand, the displacement grows unboundedly as Ω approaches Ω_{c0}. This observation reflects the fact that the mode (0, 0) is of torsional nature.

5 As the rotational speed approaches zero, the solutions for the spinning disk-stationary load system are shown, both numerically and analytically, to recover the classical solutions derived through the Airy stress function for the stationary disk-stationary load system.

It is interesting to compare the physical in-plane critical speed Ω_{in} to the physical out-of-plane critical speed Ω_{out} of a spinning disk. It is noted that Ω_{in} is independent of the thickness h of the disk,

$$\Omega_{\text{in}} = \frac{\Omega_{\text{in}}^c}{b}\sqrt{\frac{E}{\rho}},$$

where Ω_{in}^c is the lowest dimensionless in-plane critical speed. On the other hand, Ω_{out} is dependent upon the thickness (Chen, 1997),

$$\Omega_{\text{out}} = \frac{\Omega_{\text{out}}^c}{b^2}\sqrt{\frac{Eh^2}{12\rho(1-\nu^2)}},$$

where Ω_{out}^c is the lowest dimensionless out-of-plane critical speed. The ratio of these two physical critical speeds are

$$\frac{\Omega_{\text{in}}}{\Omega_{\text{out}}} = \frac{\Omega_{\text{in}}^c b}{\Omega_{\text{out}}^c h}\sqrt{12(1-\nu^2)}.$$

For a typical saw blade, we assume $b = 200$ mm, $h = 1$ mm, $\nu = 0.27$, and clamping ratio 0.5. The dimensionless critical speeds are $\Omega_{\text{in}}^c = 0.6$ and $\Omega_{\text{out}}^c = 8$, respectively (Chen and Jhu, 1996; Chen, 1997). A rough estimate based on these parameters gives us the critical speed ratio 50. In other words, in saw blade application, the out-of-plane vibration is dominant. On the other hand, in the design of spur gears and grinding wheels, the outer radius decreases while the thickness increases, say $b = 40$ mm and $h = 10$ mm. Consequently, the critical speed ratio is in the order of one. Apparently, both the in-plane and out-of-plane vibrations ought to be taken into account in these applications.

While the formulations and numerical examples presented in this paper are for a plane-stress problem, the same approach works equally well in solving a plane-strain problem with appropriate substitution in elastic constants. The corresponding plane-strain problem represents a spinning long cylinder, constrained on both ends, subject to edge loads on the outer surface with force direction perpendicular to the spinning axis and load variation independent of the axial coordinate.

References

Bhuta, P. G., and Jones, J. P., 1963, "Symmetric Planar Vibrations of a Rotating Disc," *Journal of Acoustical Society of America*, Vol. 35, No. 7, pp. 982–989.

Burdess, J. S., Wren, T., and Fawcett, J. N., 1987, "Plane Stress Vibrations in Rotating Discs," *Proceedings of Institution of Mechanical Engineers,* Vol. 201, pp. 37–44.

Chen, J.-S., 1994, "Stability Analysis of a Spinning Elastic Disk Under a Stationary Concentrated Edge Load," ASME JOURNAL OF APPLIED MECHANICS, Vol. 61, pp. 788–792.

Chen, J.-S., 1997, "Parametric Resonance of a Spinning Disk Under Space-Fixed Pulsating Edge Loads," ASME JOURNAL OF APPLIED MECHANICS, Vol. 64, pp. 139–143.

Chen, J.-S., and Jhu, J.-L., 1996, "On the In-Plane Vibration and Stability of a Spinning Annular Disk," *Journal of Sound and Vibration,* Vol. 195, No. 4, pp. 585–593.

Coker, E. G., and Filon, L. N. G., 1957, *A Treatise on Photo-Elasticity,* Cambridge University Press, London.

Doby, R., 1969, "On the Elastic Stability of Coriolis-Coupled Oscillations of a Rotating Disc," *Journal of Franklin Institute,* Vol. 288, No. 3, pp. 203–212.

Eringen, A. C., and Suhubi, W. S., 1975, *Elastodynamics,* Vol. II, Academic Press, New York.

Leung, R. C. N., and Pinnington, R. J., 1987, "Vibration of a Rotating Disc Subjected to an In-Plane Force at Its Rim, or at Its Centre," *Journal of Sound and Vibration,* Vol. 114, No. 2, pp. 281–295.

Ono, K., Chen, J.-S., and Bogy, D. B., 1991, "Stability Analysis of the Head-Disk Interface in a Flexible Disk Drive," ASME JOURNAL OF APPLIED MECHANICS, Vol. 58, pp. 1005–1014.

Shen, I. Y., and Song, Y., 1996, "Stability and Vibration of a Rotating Circular Plate Subjected to Stationary In-Plane Edge Loads," ASME JOURNAL OF APPLIED MECHANICS, Vol. 63, pp. 121–127.

Srinivasan, V., and Ramamurti, V., 1980, "Dynamic Response of an Annular Disk to a Moving Concentrated, In-Plane Edge Load," *Journal of Sound and Vibration,* Vol. 72, No. 2, pp. 251–262.

Stakgold, Ivar, 1979, *Green's Function and Boundary Value Problems,* John Wiley and Sons, New York.

APPENDIX

For the case of $n \geq 2$

$$g_{11} = -g_{21} = \kappa_{n8}\zeta^{n-1}, \quad g_{12} = -g_{22} = \kappa_{n7}\zeta^{n-1},$$

$$g_{13} = g_{23} = (1 - s_{n2})\zeta^{-n-1}, \quad g_{14} = g_{24} = (s_{n1} - 1)\zeta^{-n-1},$$

$$g_{31} = -g_{41} = \frac{\kappa_{n1}}{1 - \nu^2}, \quad g_{32} = -g_{42} = \frac{\kappa_{n3}}{1 - \nu^2},$$

$$g_{33} = g_{43} = -\frac{(n + 1)(1 - s_{n2})}{1 + \nu},$$

$$g_{34} = g_{44} = \frac{(n + 1)(1 - s_{n1})}{1 + \nu},$$

$$h_{11} = -\frac{(n + 2 + ns_{n2})\zeta^{n+1}}{4(n + 1)},$$

$$h_{12} = -\frac{[n + (2 + n)s_{n1}]\zeta^{n+1}}{4(n + 1)},$$

$$h_{13} = \frac{(n - 2 - ns_{n2})\zeta^{-n+1}}{4n(n - 1)},$$

$$h_{14} = \frac{[(n - 2)s_{n1} - n]\zeta^{-n+1}}{4n(n - 1)},$$

$$h_{21} = \frac{[n + (2 + n)s_{n2}]\zeta^{n+1}}{4(n + 1)}, \quad h_{22} = \frac{(n + 2 + ns_{n1})\zeta^{n+1}}{4(n + 1)},$$

$$h_{23} = \frac{(n + 2s_{n2} - ns_{n2})\zeta^{-n+1}}{4n(n - 1)}, \quad h_{24} = -\frac{(n - 2 - ns_{n1})\zeta^{-n+1}}{4n(n - 1)}$$

$$h_{31} = \frac{-n(1 - \nu)s_{n2} + (n - 2)\nu - n - 2}{4(1 - \nu^2)},$$

$$h_{32} = -\frac{(-n\nu + 2\nu + n + 2)s_{n1} + n(1 - \nu)}{4(1 - \nu^2)}$$

$$h_{33} = \frac{n(1 - \nu)s_{n2} + (n + 2)\nu - n + 2}{4n(1 - \nu^2)},$$

$$h_{34} = \frac{(n\nu + 2\nu - n + 2)s_{n1} + n(1 - \nu)}{4n(1 - \nu^2)}$$

$$h_{41} = \frac{\kappa_{n8}}{4(1 + \nu)}, \quad h_{42} = \frac{\kappa_{n7}}{4(1 + \nu)},$$

$$h_{43} = -\frac{1 - s_{n2}}{4(1 + \nu)}, \quad h_{44} = \frac{1 - s_{n1}}{4(1 + \nu)}.$$

For the case of $n = 1$

$$t_{11} = -t_{21} = \frac{1 + \nu}{2}, \quad t_{12} = t_{22} = -\frac{3 - \nu}{2\zeta^2},$$

$$t_{14} = t_{24} = \frac{1 + \nu}{2(3 - \nu)\zeta^2}$$

$$t_{32} = t_{42} = \frac{3 - \nu}{1 + \nu}, \quad t_{34} = t_{44} = \frac{-1}{3 - \nu}$$

$$w_{11} = \frac{(1 - 3\nu)\zeta^2}{16},$$

$$w_{12} = \frac{(1 + \nu)\ln\zeta}{4} + \frac{2(1 + \nu)(\ln\beta_{12} - \ln 2 + \gamma) - (3 - \nu)}{8}$$

$$w_{14} = w_{24} = \frac{2(1 - \nu^2)(1 + 2\ln\zeta)}{3 - \nu}, \quad w_{21} = \frac{(5 + \nu)\zeta^2}{16}$$

$$w_{22} = \frac{-(1 + \nu)\ln\zeta}{4} - \frac{2(1 + \nu)(\ln\beta_{12} - \ln 2 + \gamma) + (3 - \nu)}{8},$$

$$w_{31} = w_{41} = \tfrac{1}{8}, \quad w_{32} = w_{42} = \frac{(1 - \nu)^2}{4(1 - \nu^2)},$$

$$w_{34} = \frac{4}{3 - \nu}, \quad w_{44} = \frac{-2(1 + \nu)}{3 - \nu}.$$